Zoning in granitoid accessory minerals as revealed by backscattered electron imagery

B. A. PATERSON, W. E. STEPHENS, AND D. A. HERD

Department of Geology, University of St Andrews, St Andrews, Fife KY16 9ST, Scotland

Abstract

Accessory minerals are often difficult to investigate with light optics as the mineral grains tend to be small and the refractive indices high. Textural features due to variations in composition are well displayed in such minerals by backscattered electron imagery under circumstances designed to select only the composition contribution to electron backscattering and displayed as atomic number (Z)-contrast imagery (ZCI). It is shown by this technique that compositional zonation patterns are very common and sector zoning in titanite is described for the first time. The compositional basis for zonation of titanites in this study is shown to be controlled by coupled substitutions involving the *REE*. The technique is particularly good at revealing rounded cores to zircon grains which are normally taken to be refractory grains from the magma source region, and ZCI studies may improve targeting of grains for U–Pb geochronological investigations. Several examples are presented of applications of the technique to accessory minerals encountered in polished thin sections of granitoids in the Caledonian of Scotland. The consequences of ZCI studies for trace element modelling of *REE* in granitoid petrogenesis are discussed.

KEYWORDS: zoning, accessory minerals, backscattered electron imagery.

Introduction

ACCESSORY minerals have an influence on petrogenetic studies far greater than their abundances might suggest. This is because they are normally the principal repositories of the rare earth elements (*REE*), U, and Th. Modelling of igneous processes is often dependent on variations in *REE* abundances, and the U–Pb and Sm–Nd radiogenic isotope techniques are dependent on accessory mineral enrichment in these elements. It is important, therefore, to understand the growth histories of accessory minerals before making simple assumptions for modelling and/or geochronological purposes.

Studies of accessory minerals using light optical microscope techniques are disadvantaged by limitations of magnification. The very high refractive indices of most accessory minerals further limit the optical information observable in transmitted light; sometimes more information is available from polished and etched samples using incident light optics. Electron beam techniques reveal other types of information about accessory minerals at high magnification including composition and textural variations in single grains. The results of various electron interactions within the target are detected and displayed on a CRT screen in synchronization with the rastering of the primary electron beam on the surface of the specimen to give an image of the crystal or rock being investigated. Secondary electrons resulting from surface interactions yield primarily information on surface relief (secondary electron imagery, SEI). Backscattered electrons (BSE), on the other hand, result from the complex interplay of several factors including relief, crystallographic structure, and atomic number and this information is displayed as backscattered electron images (BEI). By isolating the composition factor it is possible to visualise the mineral in terms of variations in mean atomic number (Z-contrast image, ZCI). X-rays also result from electron interactions and provide element-specific composition information (X-ray imagery, XRI).

This paper describes the application of ZCI to the study of granitoid accessory minerals. It is our experience that most accessory minerals are not homogenous crystals but show various types of compositional variation (zonation) which are revealing about the petrogenesis of the rock. The objects of this contribution are to illustrate the

Mineralogical Magazine, March 1989, Vol. 53, pp. 55–61

capability of the ZCI technique in revealing zoning, to describe the textural types of zonation observed, and to suggest how the technique may be used to constrain petrogenetic models and to improve methods of targeting grains for isotopic studies.

Techniques

A detailed treatment of the theory of electron backscattering has been presented by Goldstein *et al.* (1981) and a review of backscattered electron techniques in mineralogy was given by Lloyd (1987). Contributions to the total BSE signal are due to composition (mean atomic number), crystallography (electron channelling) and topography (tilt angle). To suppress the crystallographic and topographic contributions flat mechanically polished microprobe slides were used, only slides with a surface produced by electro-polishing would show a crystallographic effect (Nakagawa, 1986). Thus the BSE signal produced relates directly to the mean atomic number ($\bar{Z}$) of the specimen.

The backscattered electron coefficient ($\bar{\eta}$) describes the dependence of electron backscattering on $\bar{Z}$ (the mean atomic number) of the target material, in simple compounds where the composition is controlled by just two end-members the value for $\bar{Z}$ may be unique to a composition within the solid-solution series. However, in more complex compounds where there may be several end-members or where minor element substitution is significant then the uniqueness of the value for $\bar{Z}$ may no longer hold. Thus several compositions may result in the same BSE intensity (or grey scale level in ZCI) and it is very important to check whether this is occurring.

The instrument used for the ZCI micrographs and for the point analyses was a JEOL JCXA-733 electron probe microanalyser. For the ZCI micrographs a beam of 15 kV, current of 20 nA and objective aperture of 170 μm was used. The type of backscattered electron detector fitted to a JEOL JCXA-733, and used in unmodified form in this study, is a Si, P–N junction type of divided annulus. The images of accessory minerals presented in this paper depend largely on DC suppression to allow amplification of the small differences in signal due to Z-contrast. A number of line profiles of relative $\bar{\eta}$ intensity were used to obtain an uncalibrated measure of the BSE signal.

Only WDS spectrometry of X-ray emissions is capable of resolving the *REE* at the sensitivity and spatial resolution required. The analytical procedure used was similar to that of Exley (1980); intra-*REE* interferences and those from other elements were overcome by using $L\beta_1$ peaks for Pr, Nd, and Sm, and $L\alpha_1$ for Y, La, Ce, and Yb. A beam of 20 kV, current of 50 nA and count times on peak of 60 s were used, an unrastered beam was employed analysing an area of approximately 2 μm^2. The glass standards of Drake and Weill (1972) were used as reference standards for the *REE* and apparent concentrations were corrected by standard ZAF correction methods for all measured elements.

The ZCI examples presented in this paper were all taken from standard microprobe sections from the Scottish Caledonian plutonic complexes of Cluanie, Ratagain, and Strontian (see Brown (1983) for a review of the province). None were from separates or selected for special reasons, thus emphasising the likelihood that such variations are commonplace within granitoid accessory minerals. Most grains in these sections were zoned in similar ways to those shown here. It should be emphasised that studies of other samples from these and other Caledonian plutons have shown that such textures are very widespread.

Z-contrast imagery (ZCI)—an example

Sector zoning in titanite. A single titanite crystal from a sample of appinite (BP/SR/A1, Grid Ref. NM 795 603) from within the Strontian granitoid pluton was selected from a normal electron microprobe polished thin section (i.e. not selected from a heavy mineral concentrate); all the titanite grains in this section were zoned in a similar way. The crystal (Fig. 1) shows a wide range of backscattered electron intensity and was used in a detailed study relating the intensity of electron backscattering with mineral composition. The crystal was selected because it apparently reveals several types of compositional zonation namely continuous, discontinuous and sector zoning (see next section). We believe that this is the first reported instance of sector zoning in titanites.

The relative grey levels on a ZCI micrograph (e.g. Fig. 1) reflect levels of electron backscattering and given that composition is the primary control on backscattering then each grey-level reflects the same $\bar{Z}$ value. Selected points on the crystal (Fig. 1) were analysed by WDS X-ray spectrometry. Points were selected for analysis both by traversing outwards across the continuous and discontinuous zones and at the same relative positions within adjacent sectors. The results for major elements Si, Al, Ti, Fe, Mn, Mg, Ca, and minor elements La, Ce, Pr, Nd, Sm, Yb, and Y at each point are given in Table 1. From these results values for $\bar{\eta}_c$ (the calculated backscattered electron coefficient) and $\bar{Z}$ were obtained using the method described by Lloyd (1987).

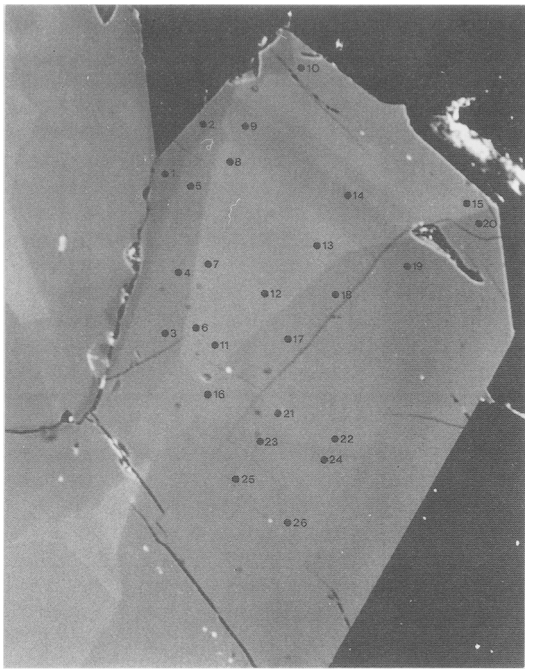

FIG. 1. Two titanite crystals showing sector, continuous, and discontinuous zoning. The analyses spots are cross referenced with the data presented in Table 1. The host rock is an appinite from within the Strontian biotite granite (BP/SR/A1, Grid Ref. NM 795 603). Width of field of view 0.2 mm.

From the compositions of the various points (Table 1) it is clear that $\Sigma(REE+Y)_2O_3$ varies more than three-fold from 1.4–4.4 wt. %. Given that the *REE* range in atomic number from 57 to 70 and that the major constituents of titanite ($CaTiSiO_5$) typically yield a mean atomic number of 14.73 then the influence of the *REE* on $\bar{Z}$ might be expected to be substantial and this is clear from Fig. 2 which relates total $REE+Y$ to $\bar{Z}$. Clearly the effects of *REE* must be coupled with substitutions in other constituents but the primary control on variations in $\bar{\eta}$ in this crystal is the abundance of the *REE*. The *REE* tend to behave coherently as illustrated by chondrite-normalized plots for six selected points representing part of the $\bar{\eta}$ range for this crystal (Fig. 3). The coherence is taken to mean that *REE* behave as a single 'heavy' component in determining $\bar{\eta}$, and in coupled substitutions with 'light' elements is the first-order control on $\bar{\eta}$. It is then reasonable to interpret grey-scale level as contouring areas of approximately the same composition. This illustrated in another way by plotting the observed backscattering coefficient ($\bar{\eta}_o$) against $(REE+Y)_2O_3$ (Fig. 4), which underlines the conclusion that for this titanite the micrograph may be interpreted as primarily reflecting the substitution of *REE*. The same conclusion holds for other titanites in our experience though verification by analysis is necessary for reasons given above.

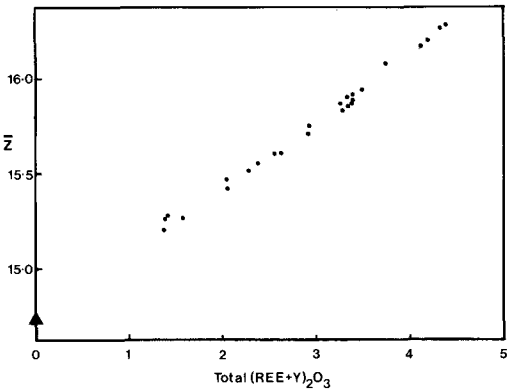

FIG. 2. Graph of mean atomic number ($\bar{Z}$) against total $(REE+Y)_2O_3$ (values are shown in Table 1). This shows the dominance of the $REE+Y$ content in determining $\bar{Z}$ and hence $\bar{\eta}$. The solid triangle is the point for pure titanite ($CaTiSiO_5$). Analyses are for the grain in Fig. 1.

Discussion. Experimental work by Green and Pearson (1986) has shown that the solubility of Ti in a melt is dependent on temperature, pressure, SiO_2 content, alkali and *REE* content, and oxygen fugacity. The stability of titanite, therefore, is dependent on Ti saturation being reached. Supersaturation in Ti may be caused by changes in any of these factors, possibly enhanced by slow diffusion of Ti in the melt. Kouchi *et al.* (1983) experimentally reproduced sector zoned clinopyroxenes in the system $CaMgSi_2O_6$–$CaTiAl_2O_6$, these experiments related elemental distribution and effective partition coefficients with growth rate which in turn was related to the degree of supercooling (or supersaturation). The results showed that within sectors elements with equilibrium partition coefficients (K_o) less than one showed an increase in content with an increase in growth rate, while elements with $K_o > 1$ showed a decrease, but between sectors, where differential growth rates exist, the opposite was true. Kouchi *et al.* (1983) concluded that interface kinetics was an essential factor in the formation of sector zoning in clinopyroxenes.

The titanite grain (Fig. 1 and Table 1) considered

Table 1. Analyses of points numbered in Figure 1.

	1	2	3	4	5	6	7	8	9	10	11	12	13
SiO_2	30.21	30.29	29.88	30.07	30.07	29.75	29.75	29.86	30.00	30.11	29.70	29.75	29.87
TiO_2	36.86	36.58	35.91	35.80	36.44	35.76	36.48	36.73	37.00	37.21	36.31	36.43	36.88
Al_2O_3	1.03	1.10	1.28	1.38	1.21	1.08	1.08	0.98	0.86	0.79	1.08	1.10	0.99
FeO	0.94	1.13	1.26	1.21	1.06	1.23	1.17	1.07	0.86	0.88	1.24	1.18	1.06
MnO	0.06	0.06	0.05	0.07	0.06	0.06	0.07	0.06	0.05	0.04	0.06	0.05	0.07
MgO	n.d.	n.d.	n.d.	n.d.	n.d.	n.d.	n.d.	n.d.	n.d.	n.d.	n.d.	n.d.	n.d.
CaO	27.56	27.51	26.55	26.53	26.97	25.73	26.46	26.82	26.71	27.10	26.53	26.38	26.68
La_2O_3	0.18	0.15	0.42	0.40	0.27	0.57	0.57	0.41	0.32	0.22	0.59	0.55	0.45
Ce_2O_3	0.62	0.64	1.48	1.35	1.03	1.81	1.89	1.43	1.18	1.03	1.83	1.86	1.51
Pr_2O_3	n.d.	n.d.	0.14	0.20	0.12	0.24	0.21	0.22	0.19	0.15	0.23	0.23	0.15
Nd_2O_3	0.41	0.41	0.83	0.85	0.65	1.22	1.12	0.90	0.64	0.52	1.28	1.08	0.97
Sm_2O_3	0.13	0.11	0.17	0.24	0.12	0.12	0.20	0.12	0.07	0.06	0.19	0.17	0.17
Yb_2O_3	n.d.	n.d.	n.d.	n.d.	n.n.	n.d.	n.d.	n.d.	n.d.	n.d.	n.d.	n.d.	n.d.
Y_2O_3	0.23	0.25	0.34	0.30	0.09	0.23	0.21	0.24	0.13	n.d.	0.22	0.20	0.13
Total	98.23	98.23	98.31	98.40	98.03	97.80	99.21	98.84	98.01	98.11	99.26	98.98	98.93
$\Sigma(REE+Y)_2O_3$	1.57	1.56	3.38	3.34	2.28	4.19	4.20	3.32	2.53	1.98	4.34	4.09	3.38
$\bar{\eta}_c$	0.1802	0.1801	0.1838	0.1836	0.1816	0.1861	0.1858	0.1840	0.1821	0.1813	0.1863	0.1856	0.1841
$\bar{Z}$	15.28	15.26	15.88	15.86	15.53	16.27	16.20	15.90	15.60	15.46	16.28	16.17	15.92

	14	15	16	17	18	19	20	21	22	23	24	25	26
SiO_2	30.04	30.06	29.63	29.69	29.97	30.20	30.21	29.81	30.06	29.92	29.96	30.01	29.98
TiO_2	37.68	37.28	36.16	36.45	36.93	37.42	37.57	35.87	36.32	35.54	35.92	35.47	36.39
Al_2O_3	0.82	0.87	1.21	1.22	1.15	1.04	1.07	1.19	1.12	1.34	1.31	1.36	1.27
FeO	0.79	0.78	1.35	1.11	1.15	0.87	0.88	1.12	0.95	1.25	1.12	1.29	1.05
MnO	0.05	0.05	0.06	0.06	0.07	0.05	0.06	0.06	0.05	0.06	0.04	0.04	0.05
MgO	n.d.	n.d.	n.d.	n.d.	n.d.	n.d.	n.d.	n.d.	n.d.	n.d.	n.d.	n.d.	n.d.
CaO	27.00	27.36	26.71	27.06	27.33	27.86	27.98	26.38	26.76	26.23	26.60	26.45	26.85
La_2O_3	0.32	0.30	0.45	0.38	0.30	0.15	0.14	0.44	0.32	0.39	0.26	0.41	0.28
Ce_2O_3	1.09	0.89	1.68	1.47	1.25	0.76	0.61	1.53	1.24	1.43	1.11	1.45	1.13
Pr_2O_3	0.16	n.d.	0.18	0.16	0.21	0.17	n.d.	0.15	0.13	0.18	0.12	0.22	0.09
Nd_2O_3	0.61	0.55	1.01	0.91	0.77	0.41	0.40	0.94	0.80	0.86	0.74	0.88	0.68
Sm_2O_3	0.06	0.07	0.20	0.10	0.11	0.03	0.09	0.17	0.12	0.13	0.14	0.15	0.13
Yb_2O_3	n.d.	n.d.	n.d.	n.d.	n.d.	n.d.	n.d.	n.d.	n.d.	n.d.	n.d.	n.d.	n.d.
Y_2O_3	0.11	0.17	0.18	0.21	0.23	n.d.	0.09	0.24	0.28	0.28	0.30	0.25	0.31
Total	98.73	98.38	98.82	98.82	99.47	98.96	99.10	97.90	98.15	97.61	97.62	97.98	98.21
$\Sigma(REE+Y)_2O_3$	2.35	1.98	3.70	3.23	2.87	1.52	1.33	3.47	2.89	3.27	2.67	3.36	2.62
$\bar{\eta}_c$	0.1820	0.1811	0.1851	0.1838	0.1831	0.1802	0.1798	0.1841	0.1827	0.1835	0.1823	0.1837	0.1821
$\bar{Z}$	15.56	15.42	16.08	15.87	15.75	15.28	15.20	15.94	15.71	15.85	15.63	15.88	15.60

$\bar{\eta}_c$ is the calculated BSE coefficient. $\bar{Z}$ is the mean atomic number. n.d. - not detected. The 97-98% totals are due to incomplete analysis, missing elements are the other REE (estimated at no more than 10% of the total REE) and other elements in trace amounts possibly including Nb, Ta, Th, U, Na and Ba.

here shows a similar distribution of elements between sectors (where relative growth rates can be evaluated), in terms of K_o values, to that found by Kouchi *et al.* (1983) in clinopyroxenes. The *REE* ($K_o > 1$) content of the fastest growing sector (analyses 6–15) is higher than that of the slowest growing sector (analyses 23–26), Al_2O_3 ($K_o < 1$) content is highest in the slowest growing sector and lowest in the fastest growing sector. We consider that growth kinetics controlled by supersaturation is an important factor in producing sector zoning in titanite. From charge and ionic radius considerations slow diffusion of Ti is probable, when this is considered the likelihood of kinetic disequilibrium existing in titanites is not surprising. In our experience such disequilibrium is common in titanites.

Zonation textures

A number of other zoning textures have been observed in the accessory minerals apart from the sector zoning described above. These are categorized in a non-genetic way and illustrated using ZCI in Figs. 1 and 5. The use of descriptive terminology is intended to be non-genetic and follows closely that of MacKenzie *et al.* (1982). Discussion of the origin of individual textures is not addressed here as the primary purpose of this paper is to illustrate that zoning textures can easily be observed using the BSE technique. It is important to note that a combination of these textures is the norm rather than the exception.

Continuous zoning. In our experience this is a common feature in accessory minerals, as it is in

many major silicate minerals. As with major phases continuous zoning is often superimposed on other types of zoning, most commonly discontinuous zoning. As illustrated here (Fig. 1 and accompanying Table 1) continuous zoning is superimposed on sector zoning.

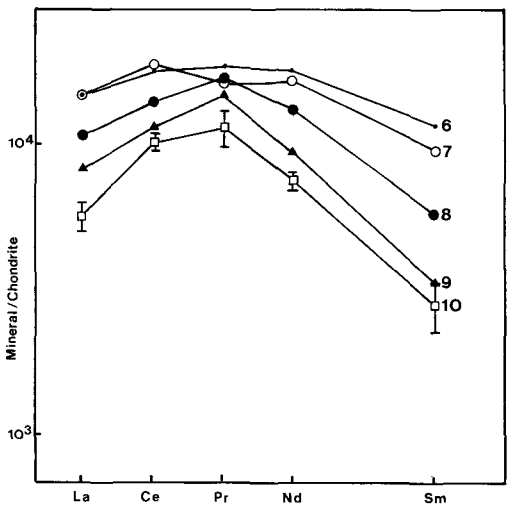

FIG. 3. Chondrite-normalized plot for five points from Fig. 1 (analyses see Table 1). These show that the *REE* in this titanite behave as a coherent group; refer to the text for details. Error bars (2σ) are shown for analysis 10.

Discontinuous zoning. This category includes multiple zoning, oscillatory zoning and convolute zoning. Again all these features are commonly seen in major mineral phases and their origin is the subject of much debate. Fig. 5*a* is a titanite with oscillatory zoning confined to the edges of the crystal, this is the most common occurrence and it is often associated with continuous zoning. Zircons also commonly show oscillatory zoning (Fig. 5*b*). Figs. 1, 5*c* and *d* also show titanite and zircon crystals which have discontinuous zoning (including the sub-types mentioned above).

Sector zoning. Sector zoning is a widely described feature found in many minerals, but is particularly common in pyroxenes in alkali-rich basic and ultrabasic rocks (Deer *et al.*, 1966). Amongst accessory minerals, sector zoning has been observed in zircons (e.g. Chase and Osmer, 1966; Fielding, 1970; Krogh, 1982; Hoffman and Long, 1984). This study reports sector zoning in titanites and zircons from Caledonian plutonic complexes; Figs. 1 (titanite) and 5*c* (zircon). We believe this to be the first reported instance of

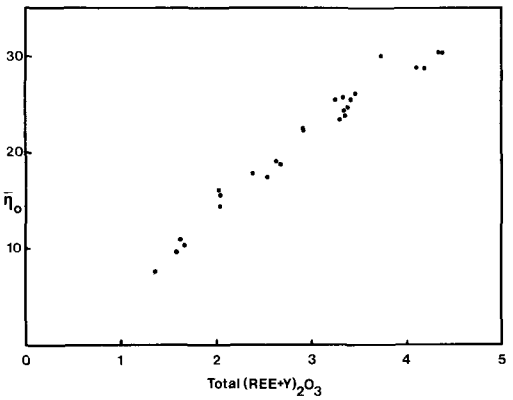

FIG. 4. Graph of observed BSE coefficient ($\bar{\eta}_o$; arbitrary scale) against total $(REE+Y)_2O_3$ for titanite. This emphasizes the fact that, in this case, the grey-levels can be considered as contouring $REE+Y$ contents. Analyses (Table 1) are from the grain in Fig. 1.

sector zoning in titanites and in our experience it is a widespread feature of a variety of igneous rocks.

Discrete cores. The presence of cores in zircons is well known, but observing them has relied on transmitted or reflected light often enhanced by etching techniques. Fig. 5*b* and *c* both show zircons with easily observed cores. Cores, in the sense of having an anhedral central portion with a sharply defined margin, have also been seen in titanite (Fig. 5*e*) and apatite (Fig. 5*f*).

Petrogenetic implications

The most important implication of zonation textures is that they limit the interpretations that are possible of accessory mineral growth histories, or indeed, any mineral where there is compositional zonation, and this places constraints on petrogenetic models. The presence of unambiguous restite in granites, in the form of zircon with older cores than overgrowths, represents a two-stage growth history. We have shown that zircon cores can easily be identified using the ZCI technique. Where isotopic evidence is lacking this technique may be used to identify possible restite by textural criteria only. It is suggested that the technique described herein might improve selection of grains for isotopic study with respect to homogeneity of both grain composition and population. Vander Wood and Clayton (1985) used ZCI to aid ion-probe targeting for U–Pb analysis. Zircons, which have been shown by the SHRIMP ion-probe (Williams *et al.*, 1984) to have old cores and young rims, give far superior

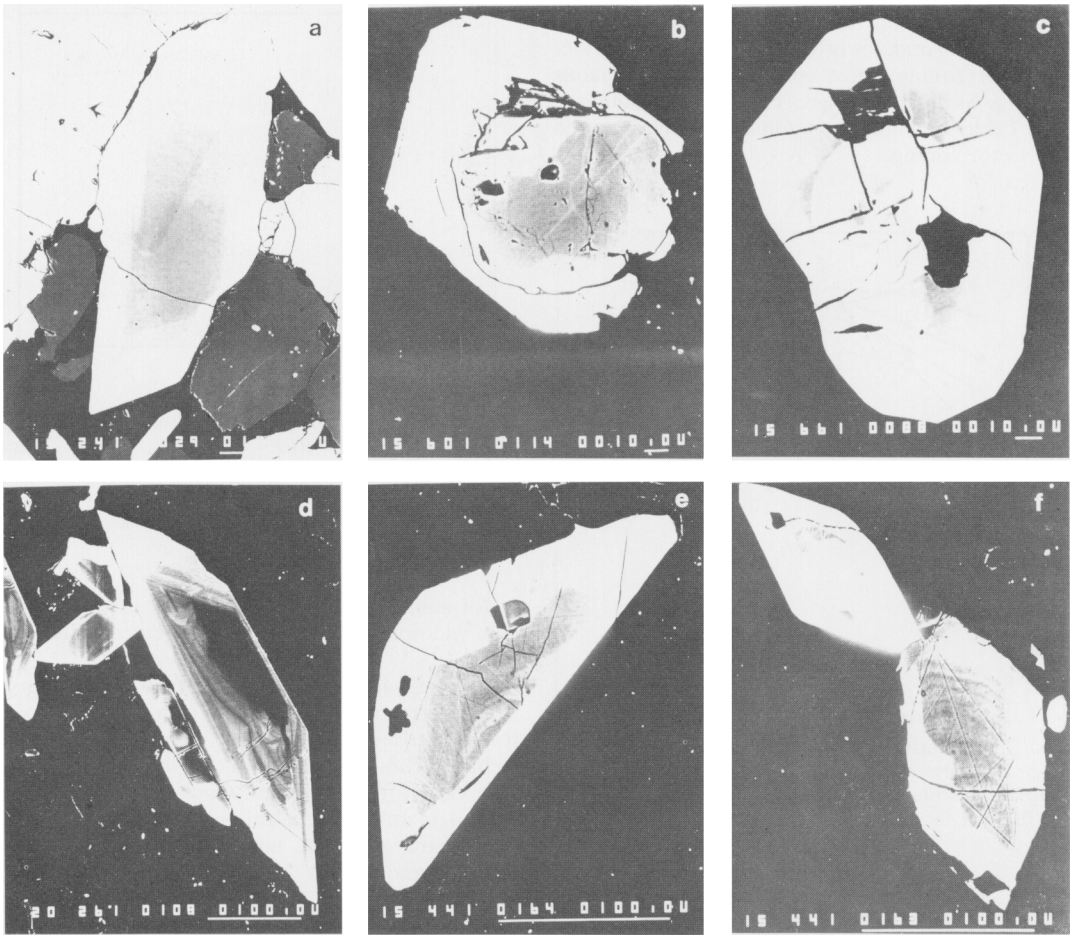

FIG. 5. (*a*) A titanite showing outer marginal oscillatory zoning. The host rock is a hornblende syenite (50% hornblende, 15% titanite, 35% K-feldspar with accessory apatite) from the Ratagain complex (RAT 56, Grid Ref. NG 886 177). Scale bar 100 μm. (*b*) A zircon with a core and overgrowth with oscillatory zoning. The core is clearly rounded and is markedly different in composition to that of the overgrowth. The host rock is a granodiorite from the Cluanie intrusion (MGW 19, Grid Ref. NH 152 078). Scale bar 10 μm. (*c*) A zircon with a rounded core and euhedral overgrowth; in addition both the core and the overgrowth show sector, continuous and discontinuous zoning. the zircon is in a diorite from the Ratagain complex (RAT 13/1, Grid Ref. NG 887 176). Scale bar 10 μm. (*d*) Shown here are a number of titanites, the largest of which has discontinuous zoning, including convolute zoning. The host rock is the same as that described in Fig. 5*a* (RAT 56, Grid Ref. NG 886 177). Scale bar 100 μm. (*e*) This shows a titanite with a clearly irregular core and a euhedral rim. Poorly defined zones within the core are cross cut by the euhedral rim. The host rock is the syenite from Ratagain described in Fig. 5*a* (RAT 56, Grid Ref. NG 886 177). Scale bar 100 μm. (*f*) An apatite with a well-defined core and euhedral rim, this texture is directly analogous to that shown in Fig. 5*e* and is from the same rock (RAT 56, Grid Ref. NG 886 177). Scale bar 100 μm.

core/rim discrimination by ZCI than by conventional light optical techniques. Because trace elements and isotopic analyses are widely used in petrogenetic modelling the interpretation of the growth histories of trace element rich accessories is of obvious importance. Any model based on trace elements and isotopes should take into consideration the possibility of restite in accessory phases. In addition to restite, many of the examples show disequilibrium textures (Figs. 1 and 5*c*), therefore the use of single mineral-melt partition coefficients in such models is a gross over-simplification and it is possible that the actual partitioning of some trace elements may be governed by kinetic

factors such as diffusivities and crystal growth rate, as discussed above.

Many of the zonation textures described in this paper are usually interpreted in major phases as being due to growth in magmatic environments (e.g. Figs. 1, 5*b* and *c*), the preservation or alteration of these textures may indicate the extent of post-crystallization changes in the accessory minerals. This is important if such changes result in the redistribution of elements used in modelling magmatic processes and it may extend the interpretation of growth histories into the subsolidus environment.

Accessory minerals have long been used in sedimentary provenance studies. Traditionally attributes such as type, habit and colour are used to characterize a source, but more recently compositional parameters have been used (Owen, 1987). Internal textures as revealed by ZCI could be added to this list where characteristic of a given provenance.

Conclusions

(1) The backscattered electron imaging technique is capable of revealing very small variations in bulk compositions, as little as 0.01 mean atomic number, and images using Z-contrast can be used to map such variations in single crystals.

(2) Most common accessory minerals in granitoids, including zircon, titanite, apatite, and allanite show internal variations in detail not observable using the light microscope.

(3) Cores, continuous, discontinuous and sector zoning features are common in zircons and titanites.

(4) Most variation in the Z-contrast in titanites shown in this study has been shown by analysis to be due to variations in *REE* abundances.

(5) The technique should be widely applicable to any area of investigation where accessory minerals are important, for instance ion-probe targeting (Vander Wood and Clayton, 1985) for U–Pb dating of zircon grains. The technique should also have a wider application in conventional U–Pb zircon studies.

(6) The ZCI technique has important implications for petrogenetic modelling and sedimentary provenance studies.

Acknowledgements

We thank Jim Allen for printing the photographs. BAP would like to thank NERC for support in the form of a NERC Studentship. Dr Ian Williams is thanked for loaning samples already dated using the 'SHRIMP' ion microprobe at the Australian National University, to allow verification that restitic cores may be recognized using ZCI. Sample MGW 19 was collected by Marc Webster. The comments of an anonymous reviewer helped improve the original manuscript.

References

Brown, P. E. (1983) In *Geology of Scotland* (G. Y. Craig, ed.) Scottish Academic Press, Edinburgh. 472 pp.

Chase, A. B., and Osmer, J. A. (1966) *J. Electrochem. Soc.* **113,** 198–9.

Deer, W. A., Howie, R. A., and Zussman, J. (1966) *An Introduction To The Rock Forming Minerals.* Longman, London. 528 pp.

Drake, M. J., and Weill, D. F. (1972) *Chem. Geol.* **10,** 179–81.

Exley, R. A. (1980) *Earth Planet. Sci. Lett.* **48,** 97–110.

Fielding, P. E. (1970) *Am. Mineral.* **55,** 428–40.

Goldstein, J. I., Newbury, D. E., Echlin, P., Joy, D. C., Fiori, C., and Lifshin, E. (1981) *Scanning electron microscopy and X-ray microanalysis.* Plenum Press, New York, 673 pp.

Green, T. H., and Pearson, N. J. (1986) *Chem. Geol.* **54,** 185–201.

Hoffman, J. E., and Long, J. V. P. (1984) *Mineral. Mag.* **48,** 513–17.

Kouchi, A., Sugawara, Y., Kashima, K., and Sunagawa, I. (1983) *Contrib. Mineral. Petrol.* **83,** 177–84.

Krogh, T. E. (1982) *Geochim. Cosmochim. Acta,* **46,** 637–49.

Lloyd, G. E. (1987) *Mineral. Mag.* **51,** 3–19.

MacKenzie, W. S., Donaldson, C. H., and Guilford, C. (1982) *Atlas of igneous rocks and their textures.* Longman, London. 148 pp.

Nakagawa, S. (1986) *JEOL News,* **24E,** 7–14.

Owen, M. R. (1987) *J. Sediment. Petrol.* **57,** 824–30.

Vander Wood, T. B., and Clayton, R. N. (1985) *J. Geol.* **93,** 251–70.

Williams, I. S., Compston, W., Black, L. P., Ireland, T. R., and Foster, J. J. (1984) *Contrib. Mineral. Petrol.* **88,** 322–7.

[*Manuscript received 25 April 1988; revised 8 June 1988*]